The International Journal of Cardiovascular Imaging (2019) 35:1407–1420
https://doi.org/10.1007/s10554-018-1448-4

REVIEW PAPER

Advanced imaging in pulmonary hypertension: emerging techniques and applications

Fabian Rengier[1,2,3] · Claudius Melzig[1,2] · Thorsten Derlin[4,5] · Alberto M. Marra[6] · Jens Vogel-Claussen[5,7]

Received: 14 June 2018 / Accepted: 24 August 2018 / Published online: 30 August 2018

Abstract

Pulmonary hypertension (PH) is a pathophysiological disorder defined by an increase in pulmonary arterial pressure which can occur in multiple clinical conditions. Irrespective of etiology, PH entails a negative impact on exercise capacity and quality of life, and is associated with high mortality particularly in pulmonary arterial hypertension. Noninvasive imaging techniques play an important role in suggesting the presence of PH, providing noninvasive pulmonary pressure measurements, classifying the group of PH, identifying a possibly underlying disease, providing prognostic information and assessing response to treatment. While echocardiography, computed tomography (CT) and ventilation/perfusion scans are an integral part of routine work-up of patients with suspected PH according to current guidelines and across centers, innovative new techniques and applications in the field of PH such as 3D echocardiography, dual-energy CT, 4D flow magnetic resonance imaging (MRI), T1 and extracellular volume fraction mapping, non-contrast-enhanced MRI sequences for perfusion and ventilation assessment, and molecular-targeted positron emission tomography are emerging. This review discusses advanced and emerging imaging techniques in diagnosis, prognostic evaluation and follow-up of patients with PH.

Keywords Pulmonary hypertension · Pulmonary circulation · Imaging

Abbreviations

mPAP	Mean pulmonary arterial pressure
CT	Computed tomography
CTEPH	Chronic thromboembolic pulmonary hypertension
CTPA	Computed tomography pulmonary angiography
DECT	Dual-energy computed tomography
ECV	Myocardial extracellular volume
FD	Fourier decomposition
FDG	18F-fluorodeoxyglucose
LV	Left ventricle
MRA	Magnetic resonance angiography
MRI	Magnetic resonance imaging
PAH	Pulmonary arterial hypertension
PET	Positron emission tomography
PH	Pulmonary hypertension
PVR	Pulmonary vascular resistance
RHC	Right heart catheterization
RV	Right ventricle
SPECT	Single photon emission computed tomography
SUV	Standardized uptake value
VMI	Ventricular mass index

✉ Fabian Rengier
fabian.rengier@web.de

1 Diagnostic and Interventional Radiology, University Hospital Heidelberg, Im Neuenheimer Feld 110, 69120 Heidelberg, Germany

2 Translational Lung Research Center (TLRC), Member of the German Center for Lung Research (DZL), University of Heidelberg, Im Neuenheimer Feld 110, 69120 Heidelberg, Germany

3 Radiology, German Cancer Research Center (DKFZ), Im Neuenheimer Feld 280, 69120 Heidelberg, Germany

4 Nuclear Medicine, Hannover Medical School, OE 8250, Carl-Neuberg-Str. 1, 30625 Hannover, Germany

5 Biomedical Research in End-stage and Obstructive Lung Disease Hannover (BREATH), Member of the German Center for Lung Research (DZL), Hannover Medical School, OE 6876, Carl-Neuberg-Str. 1, 30625 Hannover, Germany

6 IRCCS SDN Research Institute, Via Gianturco 113, 80143 Naples, Italy

7 Diagnostic and Interventional Radiology, Hannover Medical School, OE 8220, Carl-Neuberg-Str. 1, 30625 Hannover, Germany

Introduction

Pulmonary hypertension (PH) is a pathophysiological disorder defined as an increase in mean pulmonary arterial pressure (mPAP) ≥ 25 mmHg at rest as assessed by right heart catheterization (RHC) [1]. PH can occur in multiple clinical conditions and is currently classified into five major groups with similar clinical presentation, pathophysiological characteristics and treatment strategy [1]: group 1, pulmonary arterial hypertension (PAH); group 2, PH due to left heart disease; group 3, PH due to lung disease and/or hypoxia; group 4, chronic thromboembolic PH (CTEPH); group 5, PH with unclear and/or multifactorial mechanisms. Irrespective of etiology, PH entails a negative impact on exercise capacity and quality of life, and is associated with high mortality despite therapy, particularly for patients with PAH. Persistent elevation of mPAP may lead to irreversible remodeling of the pulmonary vasculature and eventually right heart failure [2, 3]. Prognosis can be improved by early diagnosis and initiation of the appropriate treatment.

Imaging aims at suggesting the presence of PH, providing noninvasive pulmonary pressure measurements, classifying the group of PH, identifying a possibly underlying disease, providing prognostic information and assessing response to treatment. This review discusses emerging imaging techniques and applications in diagnosis, prognostic evaluation and follow-up of patients with PH. The review focusses on emerging techniques which are on the verge of being integrated into clinical routine or which have the potential to aid clinical decision making in the future.

Imaging modalities

Echocardiography

Trans-thoracic echocardiography (TTE) plays a pivotal role in the screening and diagnostic algorithm of PH [1]. Pulmonary artery systolic pressure (PASP) is estimated by measuring maximal tricuspid regurgitation velocity, applying the modified Bernoulli equation and adding estimated right atrial pressure. Nonetheless, tricuspid regurgitation velocity measurements are only trustworthy when a good Doppler signal is available [4]. Besides, the DETECT study showed that a PAH diagnosis associated with systemic sclerosis cannot rely on echocardiography alone [5].

Furthermore, TTE allows for the assessment of right heart morphology and function which is crucial for therapy monitoring and risk assessment. Marra et al. demonstrated that patients treated with Riociguat experienced a reduction in right heart size and improvement of systolic function [6]. The increase in right ventricular (RV) endsystolic and enddiastolic volume during follow-up has been shown to predict treatment failure [7]. Additionally, pericardial effusion independently predicts outcomes in PAH, whereas its resolution is associated with better prognosis [8]. Echocardiography may help to stratify the risk of PAH patients based on right atrial area and the presence or absence of pericardial effusion [9, 10]. In addition to resting echocardiography, exercise-induced increase of PASP is associated with worse prognosis [11].

The complex shape of the RV complicates its evaluation. Indeed, three distinct segments are detectable in the RV: the inflow region, the outflow tract, and the apical region [12]. For this reason, guidelines recommend to perform measurements and evaluation in different views [13]. The 3D reconstruction of the RV shape based on 2D images is a new and promising technique that might help assessment of the complex geometry of the RV [14]. The 3D reconstruction of the RV shape is performed offline and may require up to 5 min after the acquisition of the 2D images. Modern equipment enables an automatic correction of border detection through dedicated algorithms. 3D echocardiography has been shown to provide an accurate estimation of RV volume and RV ejection fraction, taking cardiac magnetic resonance imaging (MRI) as a gold standard [15, 16]. However, several issues still limit 3D echocardiography of the RV, in particular its load dependency, its accuracy when interventricular changes affecting septal motion are present, poor acoustic windows and irregular rhythm [17]. Moreover, 3D reconstruction often is not reliable in patients with severely enlarged RV [18].

Strain imaging is another recently developed technique that might help physicians in PH diagnosis and follow-up [19]. Strain and strain rate index reflect RV myocardial deformation and the speed at which this deformation occurs, respectively, through the use of speckle tracking (Fig. 1) [20]. The reduction of the RV myocardial deformation indicates the extent of the PH severity [21]. Moreover, the assessment of RV longitudinal strain (specifically an RV longitudinal strain ≥ 19%) predicts all-cause mortality [22]. However, strain techniques are still burdened by several limitations, especially the lack of standardization of the method and of the used software. Another major limitation it is its volume-load dependency [22, 23]. The latter might be overcome by a new technique, RV automated systolic index, which is angle-independent and requires low frame rate image acquisition [24].

Combining 3D echocardiography and strain imaging might be a powerful tool to predict RV failure and outcomes in PAH patients [25]. Both techniques are

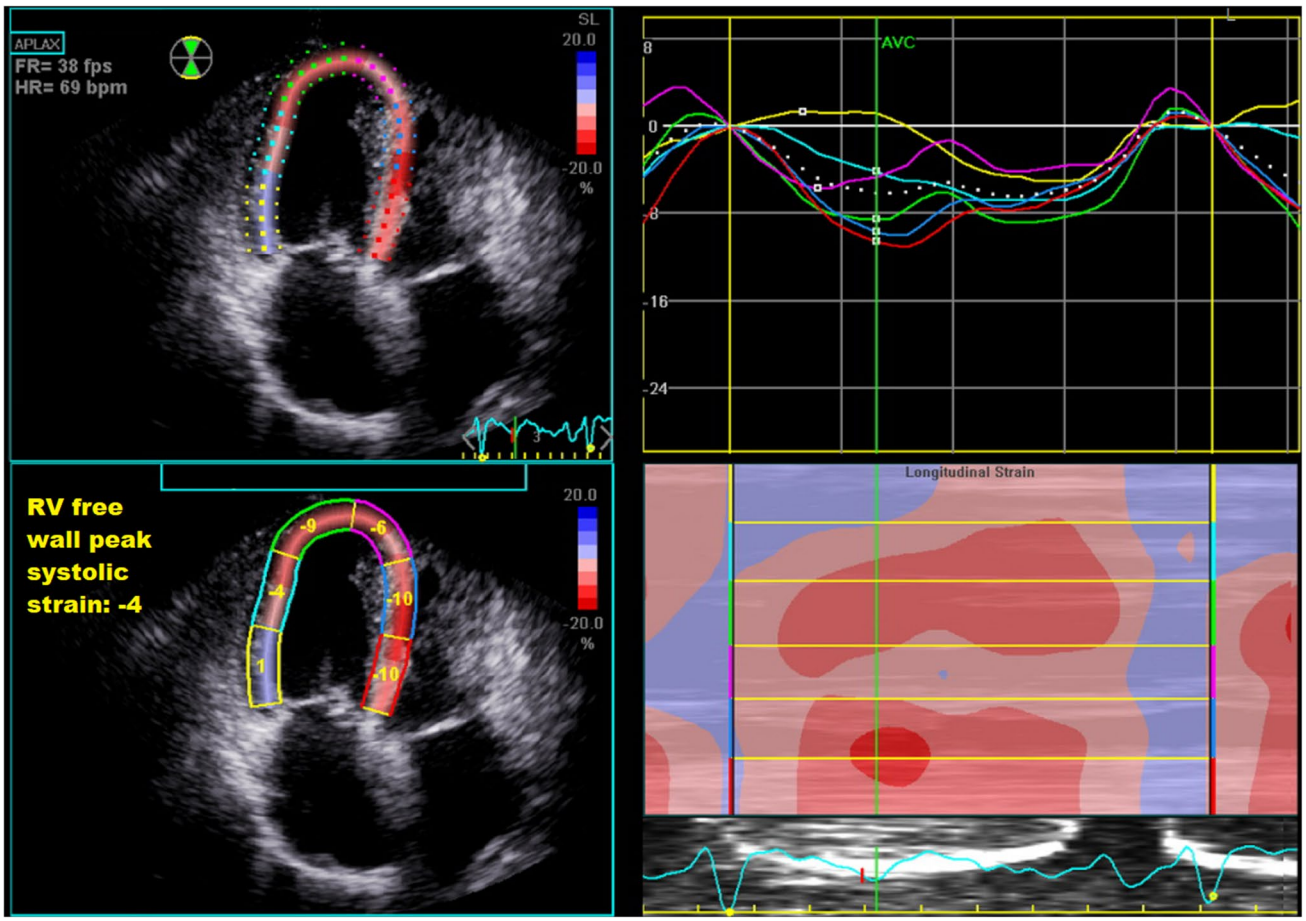

Fig. 1 Echocardiographic strain imaging in a patient with severe pulmonary arterial hypertension and enlarged right heart. Top left image shows a 4-chamber view used to assess right ventricle (RV) longitudinal speckle tracking strain. Bottom left image demonstrates the average of the basal, middle, and apical lateral peak systolic strains along the entire RV (RV free wall peak systolic strain: − 4%, normal values < 20%). The global RV longitudinal strain might be obtained considering also the septal segments. Top right image illustrates the evaluation of myocardial displacement and asynchrony of the six visible wall segments. Bottom right image shows a bull-eye view for a global overview from the apex

promising tools in the management of PH but further developments are warranted.

Computed tomography

Diagnosis of pulmonary hypertension

Computed tomography (CT), either non-contrast-enhanced CT or contrast-enhanced CT pulmonary angiography (CTPA), is frequently clinically indicated and performed in patients presenting with dyspnea, fatigue or palpitations even before the diagnosis of PH is considered by the referring physician. In this setting, the CT may be the first modality to suggest the diagnosis of PH. Features indicative of PH include a transverse pulmonary artery diameter > 29 mm in adults and a pulmonary artery to ascending aorta diameter ratio > 1 [26–28]. However, these parameters provide only moderate sensitivity and specificity for the prediction of PH [27, 29, 30].

For CTPA, typically 50–80 ml of iodinated contrast medium are injected via an antecubital vein at 4–5 ml/s followed by a saline chaser. The optimal time to start the scan is determined by either bolus tracking or test bolus techniques [31]. The patient should be instructed with respect to the inspiratory breath-hold before the actual scan to avoid rapid inspiration and Valsava maneuver [32]. With advanced image processing techniques it has become possible to extract three-dimensional quantitative parameters of pulmonary arteries from the same CTPA data. Computation of three-dimensional quantitative parameters requires three-dimensional segmentation which can be performed of both intrapulmonary vessels and central pulmonary arteries (Fig. 2). Several studies have indicated the potential of these techniques to provide higher diagnostic accuracy and better estimation of mPAP compared to one-dimensional diameter

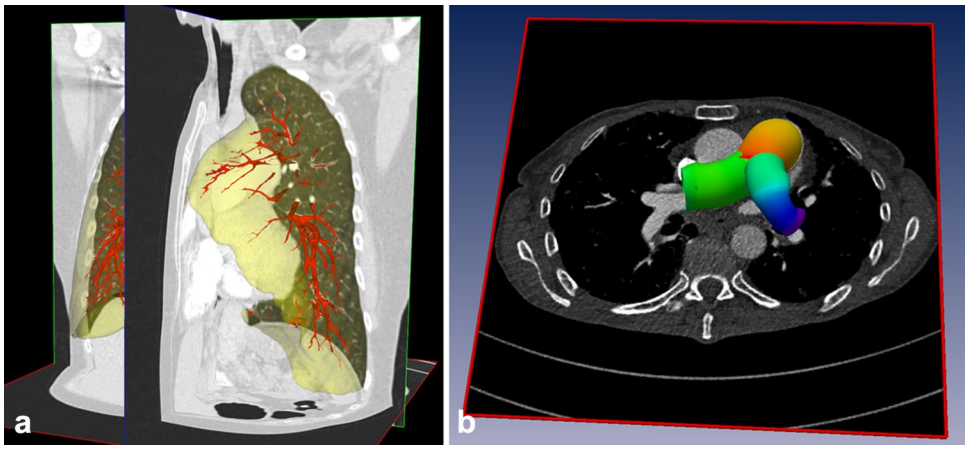

Fig. 2 **a** 3D segmentation result of intrapulmonary vessels (red) in a patient with PH. Lungs are visualized in yellow color. **b** 3D segmentation result of central pulmonary arteries with color-coding of diameter in a patient with PH

measurements, but further studies are warranted to proof this concept [33–36]. Considering that CT is performed in many of the patients with suspected PH either as part of the diagnostic work up for the presenting symptoms even before PH is suspected or as part of the diagnostic algorithm for suspected PH, noninvasive prediction of PH based on CT appears to be a promising approach for translation into clinical routine.

Classification of pulmonary hypertension

Computed tomography is also useful in classifying the form of PH. CT can identify the underlying disease, in particular parenchymal lung diseases and systemic diseases with manifestations in the lung parenchyma. Additionally, CTPA forms an integral part of the diagnostic algorithm of CTEPH for assessment of thrombus, vascular webs and stenosis to determine the treatment strategy and the suitability for pulmonary endarterectomy [1]. Left heart disease, however, may be difficult to detect by visual assessment of CTPA in the absence of features of previous cardiac surgery or cardiac decompensation. Quantification of the maximal axial cross-sectional area of the left atrium by either manual delineation or automatic segmentation allows diagnosis of left heart disease in patients with confirmed PH with good diagnostic accuracy [37, 38]. Advanced image processing techniques enable automatic segmentation and quantification of the total volume of the left atrium with possibly higher diagnostic accuracy compared to the axial cross-sectional area [39].

Assessment of pulmonary hypertension by dual-energy computed tomography

Dual-energy computed tomography (DECT) allows for calculating the iodine concentration in each voxel resulting in iodine maps as a surrogate for the lung perfusion with good agreement to pulmonary perfusion scintigraphy [40]. These iodine maps are particularly useful in evaluation of patients with CTEPH typically exhibiting triangular peripheral defects similar to perfusion scintigraphy [40]. Such functional information together with the morphological information may improve sensitivity in the diagnosis of CTEPH [41]. In CTEPH patients, iodine maps can also be used to assess response to pulmonary balloon angioplasty [42].

In addition to that, iodine maps might be helpful in the diagnosis of PAH showing less defined, nonsegmental defects [41]. The amount of such heterogeneities seems to correlate with the disease severity [43]. Finally, another useful application of DECT is the possibility of increasing the opacification of pulmonary arteries by virtual monoenergetic reconstructions in cases of inadequate contrast in the normal reconstructions [44].

Magnetic resonance imaging

Magnetic resonance imaging (MRI) provides comprehensive structural and functional assessment of the heart and the pulmonary circulation [45]. Although MRI is not integrated in the diagnostic algorithms in the 2015 ESC/ERS guidelines for the diagnosis and treatment of PH, the guidelines already point out the value of MRI for particular situations, especially for prognostic assessment and evaluation of suspected CTEPH [1]. An increasing role of MRI in the diagnosis, prognostic evaluation and follow-up can be anticipated for the near future. The following paragraphs will highlight established and emerging cardiopulmonary MRI techniques for biventricular function quantification, treatment monitoring, prognostication and regional lung function assessment in patients with pulmonary hypertension.

Cine MRI

Cine balanced steady-state free precession (SSFP) imaging belongs to any routine cardiac MRI protocol. It provides more accurate assessment of ventricular morphology and function than echocardiography [46, 47]. Right ventricular

(RV) and left ventricular (LV) end-diastolic and end-systolic volumes can be quantified from which ejection fraction and stroke volume can be calculated [45]. MRI measurements reflecting right ventricular structure and stiffness of the proximal pulmonary vasculature are independent predictors of outcome in PAH [48]. Increased RV volumes and reduced RV ejection fraction are predictive of worse outcome in patients with PAH [49, 50]. Furthermore, cine MRI allows for computation of the right and left ventricular myocardial mass from which the ventricular mass index (VMI = RV mass/LV mass) can be determined.

Cardiac cine MRI has been shown to be well suited for treatment monitoring as MRI-derived RV function improves and RV mass decreases with medical treatment of PAH [51]. Additionally, flattening of the interventricular septum can be quantified using cine MRI and is associated with the presence of PH (Fig. 3) [52]. Cine cardiac MRI derived VMI and interventricular septal angle measurements facilitate a good noninvasive pulmonary pressure estimate in PH patients as shown by Swift et al. and are ready to be used in the clinical routine [53, 54].

Emerging cine cardiac MRI techniques include advanced imaging acceleration techniques such as compressed sensing or radial sampling trajectories, three-dimensional sequences with respiratory navigation, and free-breathing sequences for real-time assessment [51].

Strain analysis

Myocardial strain can be analyzed by means of several different MRI sequences, the most-studied techniques being myocardial tagging or more recently feature tracking [55, 56]. The techniques enable analysis of regional myocardial function that may precede measurable changes in RV volumes and global function such as ejection fraction [57]. However, further studies are warranted to investigate the value of the technique in clinical practice [58].

2D and 4D flow MRI

Blood flow of the pulmonary arteries can be visualized and quantified by means of phase contrast MRI. A number of studies investigated two-dimensional phase contrast MRI

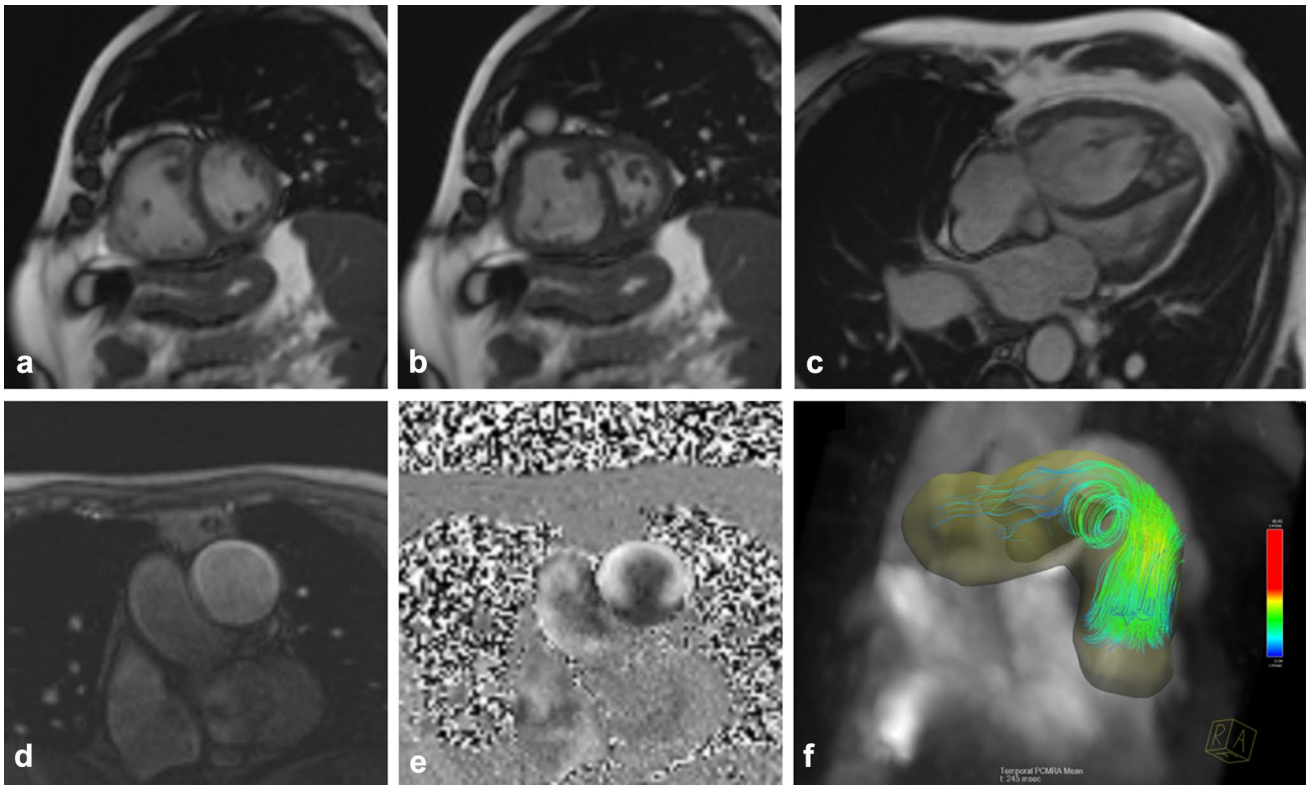

Fig. 3 64 year-old male patient with severe pulmonary arterial hypertension. **a**–**c** Cine MRI images in late diastole (**a**, short axis view) and late systole (**b**, short axis view; **c**, four-chamber view) demonstrate bowing of the interventricular septum towards the left ventricle during systole. **d, e** 2D flow MRI of the main pulmonary artery in late systole (**d**, magnitude image; **e**, phase image) exhibits heterogeneous blood flow with retrograde flow along the posterior wall and in the lumen center. (**f**) Streamline visualization of 4D flow MRI in late systole shows vortical flow in the distal main pulmonary artery

with through-plane velocity encoding in patients with PAH and detected alterations of blood flow velocities, antegrade and retrograde flow volumes and distensibility of the main pulmonary artery (Fig. 3) [51]. Four-dimensional phase contrast MRI (4D flow MRI) with three-directional velocity encoding enables a more thorough analysis of three-dimensional flow phenomena and computation of secondary flow parameters like wall stress and pressure maps [59–61]. One of the three-dimensional flow phenomena observed in PH is the occurrence of vortical flow in the main pulmonary artery, and the duration of such vortices is positively correlated with mPAP (Fig. 3) [62]. Although the clinical utility of 2D and 4D flow MRI in PH is still unclear, these techniques advance the understanding of complex pathophysiological changes occurring in the course of the disease and as a response to therapy.

Flow MRI may also be used as patient specific boundary condition for computational fluid dynamics (CFD) [63, 64]. CFD allows investigation of wall shear stress load and distribution with the pulmonary arterial tree which might relate to the disease severity of PH [65].

Delayed enhancement MRI

The technique for delayed enhancement MRI involves intravenous injection of gadolinium chelate contrast material (0.1–0.2 mmol/kg) followed by a cardiac-gated T1-weighted pulse sequence 10–15 min after contrast administration [66]. Delayed enhancement is typically seen in the anterior and posterior right ventricular insertion sites to the interventricular septum of PH patients (Fig. 4) [67–69]. Total delayed enhancement mass correlates with the degree of RV functional and hemodynamic impairment. This suggests that the amount of delayed enhancement at the RV attachment sites is directly related to the degree of RV remodeling in response to increased afterload [67, 68, 70]. McCann et al. identified areas of fibrosis, extracellular expansion and edema at the RV septal insertions at autopsy of two PH patients [71]. However, the pattern of delayed enhancement is not entirely specific and can be seen in other clinical situations leading to increased right heart volume or pressure load such as congenital heart disease for example.

T1 and extracellular volume fraction mapping

Right ventricle dysfunction in PH is not only an indicator of disease severity but also the most important predictor of survival [72]. There is a growing literature for T1 mapping of the LV, and the myocardial extracellular volume (ECV) fraction determined with this technique has been shown to correlate with histologic fibrosis [73–75]. Using an accelerated and navigator-gated Look-Locker imaging for cardiac T1 estimation (ANGIE) [76], providing high spatial resolution T1 maps in free breathing, Metha et al. could show that RV-ECV represents a unique parameter describing RV structure. RV-ECV was independently associated with both RV ejection fraction and RV end diastolic volume in PH patients [77]. Increased ECV has been found especially at the RV insertion points in patients with PH [78, 79]. In pigs with chronic PH (generated by surgical pulmonary vein banding), native T1 and ECV values at the RV insertion points were both significantly higher in banded animals than in controls and showed significant correlation with pulmonary hemodynamics, RV arterial coupling, and RV performance. ECV values also increased before overt RV systolic dysfunction, offering potential for the early detection of myocardial involvement in chronic PH useful for treatment monitoring [79].

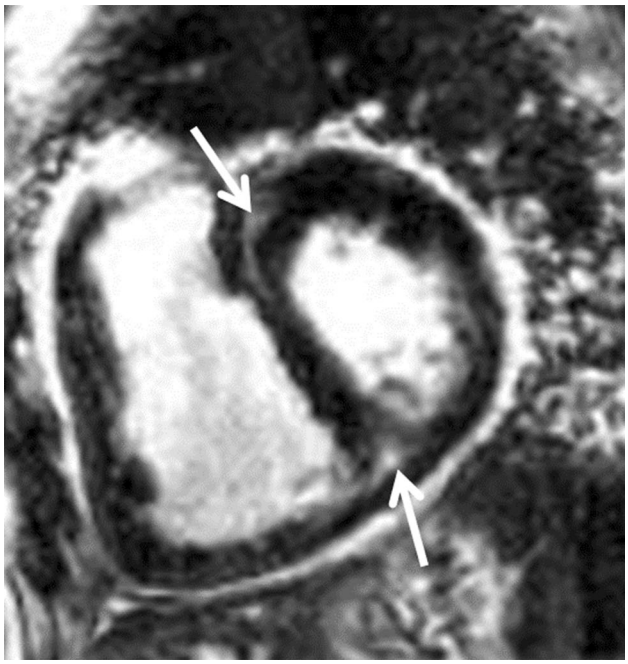

Fig. 4 61 year-old female patient with scleroderma associated PAH. Short axis myocardial delayed enhancement MRI shows delayed enhancement at the anterior and posterior right ventricular insertion sites at the left ventricular septum (arrows)

Static and time-resolved contrast-enhanced MRA

Currently, there are mainly two options to depict the pulmonary vasculature using i.v. contrast-enhanced MRA: breathhold, static, i.e. non-time-resolved 3D MRA and time-resolved (4D) MRA. While 3D MRA has typically a higher spatial resolution and is acquired in a 15–20 s breathhold, time-resolved MRA depicts the first-pass perfusion dynamics of i.v. contrast media through the lung parenchyma. Both techniques have been evaluated for the assessment of acute pulmonary emboli and CTEPH (Fig. 5). Blood pool

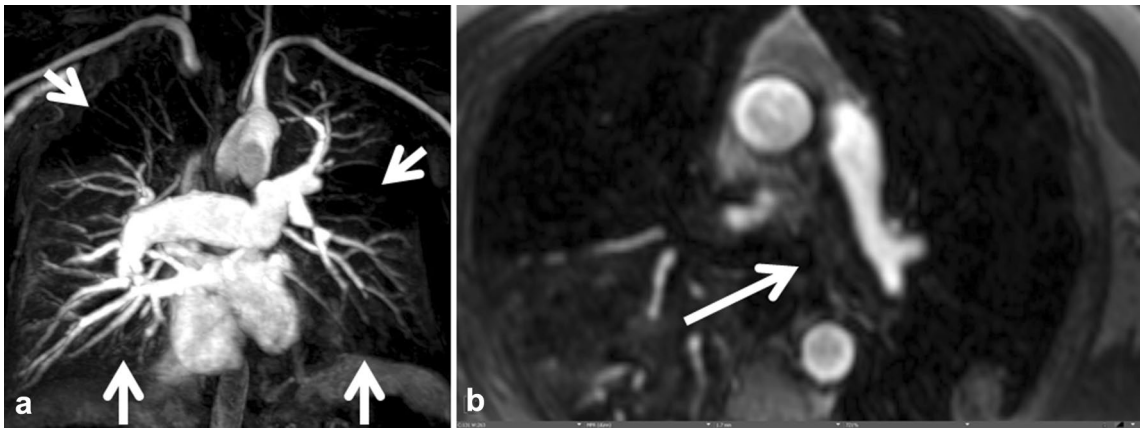

Fig. 5 63 year-old patient with CTEPH. Maximum intensity projection of the subtracted, inspiratory breathhold, contrast-enhanced 3D MRA **a** and a transverse 3D gradient-echo sequence after contrast administration **b** show chronic emboli and bands in the pulmonary arteries (arrows) in all lobes

contrast agents such as Gadofosveset might be used to perform sequential MRA of the pulmonary arteries and MR phlebography of the lower extremities after a single contrast agent injection, particularly in the setting of acute pulmonary embolism [80].

Prospective Investigation of Pulmonary Embolism Diagnosis III (PIOPED III) was a multicenter study designed to assess the efficacy of contrast-enhanced MRA for diagnosing pulmonary embolism. They found that contrast-enhanced MRA was technically inadequate in 25% of their studies and that contrast-enhanced MRA had a sensitivity of 78%, and a specificity of 99% [81]. The two major reasons for this high rate of technical inadequacy were a strict definition for complete visualization of the subsegmental pulmonary arteries and the fact that some centers were just not as good as others in producing high quality studies [82]. Based on their findings, the authors recommended that contrast-enhanced MRA should only be considered at those centers that had a sufficient technical expertise and in those patients for whom standard tests were contraindicated [81].

Chronic thromboembolic pulmonary hypertension occurs when pulmonary hypertension develops often in association with an inciting venous thromboembolic event [83, 84]. Estimates for the risk of development of CTEPH after a venous thromboembolic event range from 0.1 to 3.8% [83, 84]. Time-resolved contrast-enhanced MRA has been found to be superior to CT for assessment of therapeutic effect in CTEPH patients [85]. The strength of time-resolved contrast-enhanced MRA is its capability to fully quantify pulmonary parenchymal blood flow using deconvolution models [86, 87]. In a study by Schoenfeld et al. a combined cardiac MRI and time-resolved MRA exam was able to show detailed treatment response evaluation before and 2 weeks after pulmonary endarterectomy in CTEPH patients. In this study, the percentage change in pulmonary blood flow in the lower lobes as well as the percentage change in interventricular septal angle correlated with the percentage change in the 6 min walk test 6 months after pulmonary endarterectomy [88].

Non-contrast-enhanced MRI

Recent work has shown gadolinium deposition in the brain, skin and bones of patients with normal renal function [89, 90]. The association between the tissue deposition of gadolinium from gadolinium-based contrast agents and any short or long-term clinical importance remains to be determined [91]. However, this debate has spurred the development and use of non-contrast MRA and perfusion techniques. Moreover, non-contrast-enhanced MRI techniques are useful in patients with severe renal insufficiency [92].

The high contrast to noise of the blood pool with a steady state free precession sequence means that it can serve as a non-contrast-enhanced MRA when performed in 3D breathhold [93]. Recent developments with 3D UTE SSFP also hold promise [94]. Fourier decomposition (FD) MRI uses a continuously acquired two-dimensional steady-state free-precession (SSFP) or fast low angle shot (FLASH) acquisition [95, 96]. Since lung signal changes with respiratory and cardiovascular motion during tidal volume free breathing and during the cardiac cycle, both result in periodic changes of lung parenchymal signal at different frequencies that can be separated by means of Fourier decomposition. This results in ventilation and perfusion maps without any contrast agent. Further promising new developments of this technique using self-gated non-contrast-enhanced functional lung imaging (SENCEFUL) or phase-resolved functional lung (PREFUL) MRI have been reported [96, 97]. In principal, this technique is validated and has the potential to replace V/Q scans [98, 99]. In a single center study,

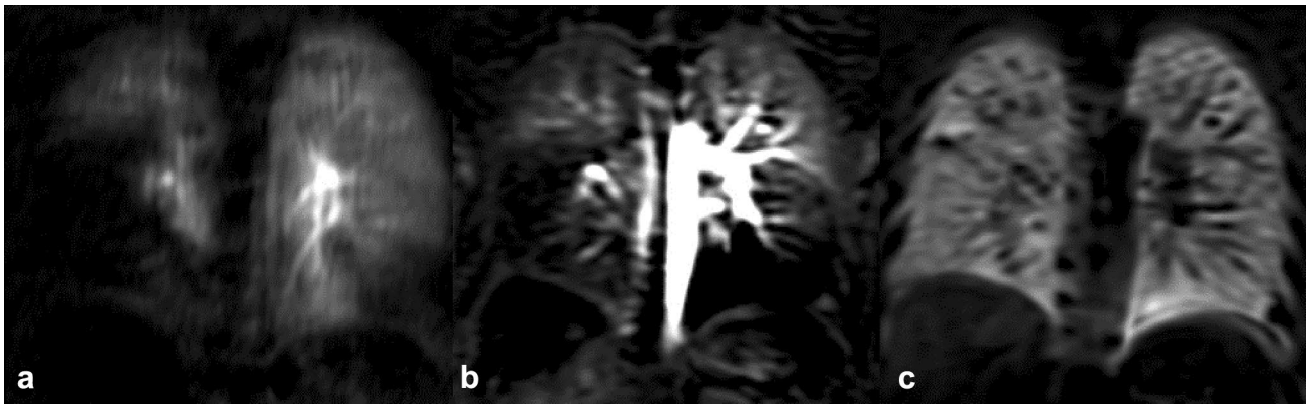

Fig. 6 45 year-old female patient with CTEPH. **a** 4D time resolved contrast-enhanced MRA shows notable bilateral lower lobe hypoperfusion due to chronic pulmonary emboli. **b** Corresponding (non-contrast) Fourier decomposition (FD) perfusion. **c** Ventilation-weighted FD MR images also depict bilateral lower lobe hypoperfusion and normal ventilation (VQ mismatch)

perfusion weighted FD MRI showed encouraging results for the diagnosis of CTEPH (Fig. 6) [100].

Nuclear medicine imaging

V/Q scans

V/Q scans, assessing both lung perfusion and ventilation, are the examination of choice in evaluating for CTEPH and differentiating CTEPH from other causes of PH, and should be obtained in all patients with PH. V/Q scanning demonstrated a sensitivity of 90–100% and specificity of 94–100% for differentiation between CTEPH and other causes of PH [101]. A normal scan essentially excludes the diagnosis of CTEPH. V/Q scintigraphy is more sensitive than multi-detector CT pulmonary angiography (CTPA) in detecting chronic thromboembolic pulmonary disease amenable to surgery, with V/Q scans demonstrating a sensitivity of 96–97.4% and a specificity of 90–95%, compared with a sensitivity of 51% and specificity of 99% for CTPA [102]. Three-dimensional single photon emission computed tomography (SPECT) is more sensitive than planar scanning for detecting vascular obstruction in CTEPH. Hybrid SPECT/CT (Fig. 7) allows assessment of both perfusion and lung anatomy, provides increased sensitivity and specificity for diagnosing pulmonary embolism [103], and may be used to quantify the extent of pulmonary perfusion defects in CTEPH [104]. Low-dose CT may also be used to obtain additional CT characteristics of PH, e.g. to establish the value of the main pulmonary artery diameter which predicts presence of PH [105].

PET scans

Pulmonary hypertension is associated with a metabolic shift towards anaerobic glycolysis in both myocardium and

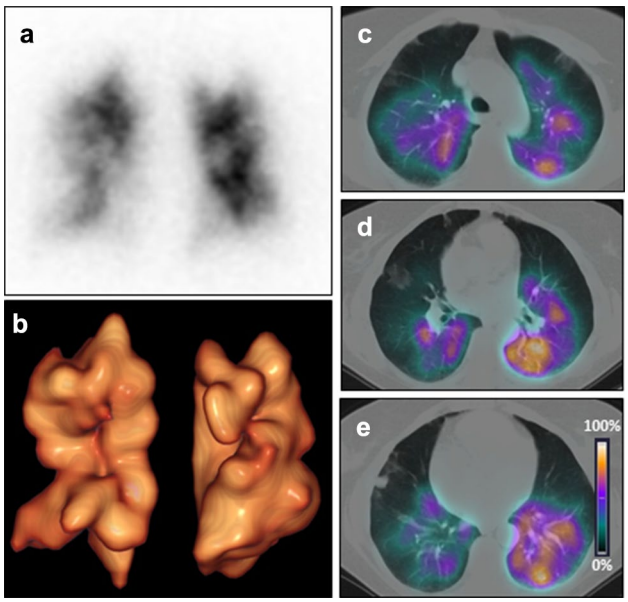

Fig. 7 Q scan. Planar perfusion image in anterior view (**a**), 3D-surface projection image (**b**) and fused SPECT/CT images showing extensive perfusion defects in both lungs in an 80-year-old female patient with CTEPH (**c**–**e**)

lung tissue, and PET may be applied to non-invasively obtain information about the metabolic state of these organs (Fig. 8). The rate of RV myocardium glucose utilization is significantly increased in PH patients compared with controls, and is significantly associated with mean pulmonary artery pressure, pulmonary vascular resistance (PVR), RV Tei index, and plasma NT-proBNP levels, and negatively correlated with RV ejection fraction [106–108]. Kluge et al. observed increasing RV-to-LV ratios of ^{18}F-fluorodeoxyglucose (FDG)-uptake with a rising PVR. Interestingly, they also found that the metabolic rate of

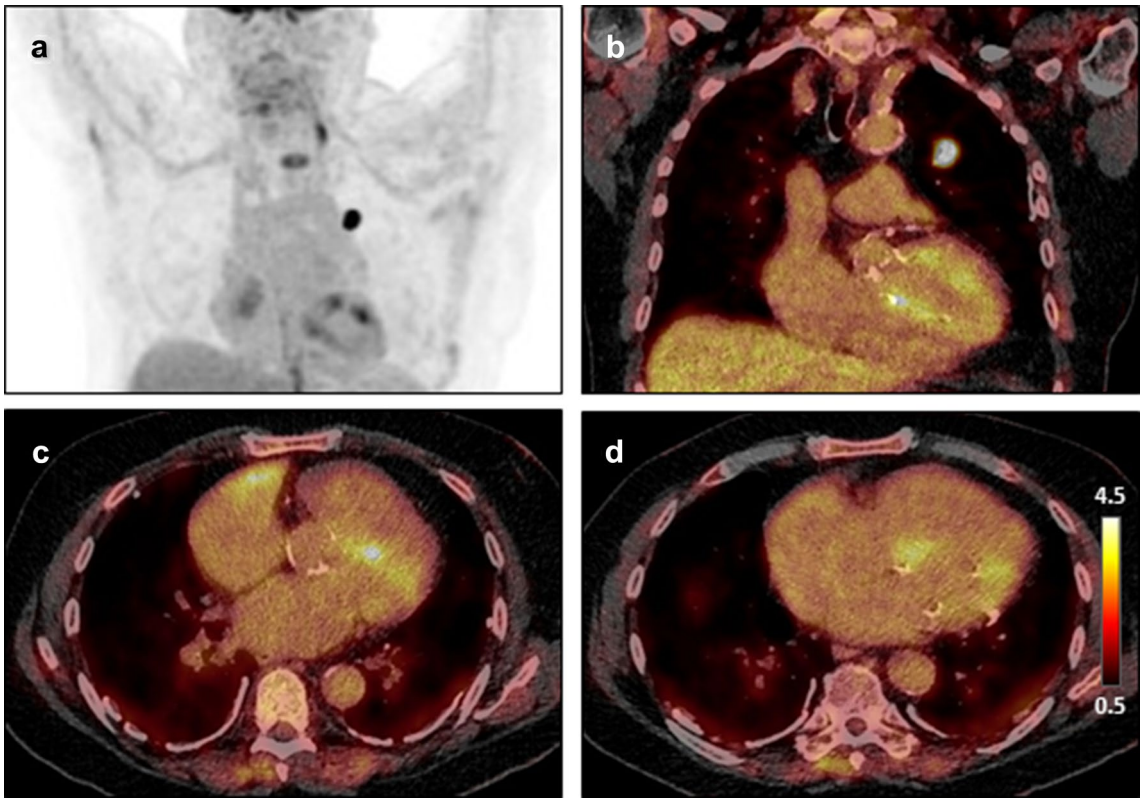

Fig. 8 ^{18}F-FDG PET/CT. PET maximum-intensity-projection image (**a**) and fused coronal and axial PET/CT images (**b, c**) showing patchy, increased glucose metabolism (SUV_{max} 6.2) in the left ventricular myocardium (physiological finding), but not in the free right ventricular wall (SUV_{max} 2.3) in an 81-year-old male patient with pulmonary hypertension and lung cancer (**d**)

glucose uptake of the left ventricle decreased ($r = -0.547$; $p < 0.01$) together with LV stroke work ($r = -0.838$; $p < 0.001$) with increasing PVR [109].

Right ventricle FDG accumulation can also be used to obtain information about the clinical outcome of PH patients. In a longitudinal study on PH patients with a mean follow-up period of 69 ± 49 months, RV FDG accumulation was significantly higher in the group that showed clinical worsening compared with the non-clinical-worsening group (10.1 vs. 7.6, $p = 0.02$). RV standardized uptake value (SUV) was significantly correlated with the time to clinical worsening (hazard ratio 1.25, 95% confidence interval 1.04–1.51, $p = 0.02$), and patients with RV-SUV ≥ 8.3 had poor prognosis compared with those with RV-SUV < 8.3 (log-rank $p = 0.005$ for time to clinical worsening and $p = 0.07$ for mortality) [110].

Moreover, RV FDG accumulation can also be used to evaluate the response to treatments. The RV FDG accumulation was attenuated after the treatment with the prostaglandin epoprostenol in accordance with the degree of reduction in the PVR and RV peak-systolic wall stress [107]. In another study, RV FDG uptake decreased as PVR decreased in patients receiving effective sildenafil treatment [111].

In addition, significantly increased lung glucose metabolism can be found in patients with PH [108, 112]. Lung metabolism varied within the PH population and within the lungs of individual patients, consistent with the recognized heterogeneity of vascular pathology in this disease, and could be attenuated by effective pharmacological treatment [112]. A recent study elucidated the nature of FDG accumulation in PAH patients, and found that HIF-1α-mediated Glut1 up-regulation in proliferating vascular cells accounts for increased lung FDG-PET uptake [113].

Besides ^{18}F-FDG, other radiotracers targeting fatty acid utilization may be used to obtain a more complete picture of substrate utilization alterations. Increased pulmonary arterial pressures are associated with increases in the ratio of ^{18}F-FDG/^{18}F-fluoro-6-thioheptadecanoic acid (FTHA) uptake in the RV. The inverse correlation between uptake and RV function may reflect a shift towards increased fatty acid oxidation and glycolysis associated with RV failure in maladaptive remodeling [114].

In summary, PET imaging has an evolving role in PH. It may provide insight into the underlying molecular biology in PH beyond morphologic imaging, provide prognostic information and evaluate the response to treatments. Although providing unique molecular information regarding

Table 1 Overview of clinical applications

	Diagnosis and classification	Prognostic evaluation	Treatment monitoring	Understanding pathophysiology
Echocardiography				
Transthoracic echocardiography	+++	+++	+++	T
3D echocardiography	T	T	T	T
Strain imaging	T	T	T	T
Computed tomography (CT)				
Routine CT	+++	++		
3D processing of CT	T	T	T	
Dual-energy CT	++	++	++	
Magnetic resonance imaging (MRI)				
Cine MRI	++	++	++	T
Strain Analysis	T	T	T	T
Flow MRI	T			T
Delayed enhancement MRI		++		
T1 and extracellular volume fraction mapping		T	T	T
Contrast-enhanced MRA	++		+	
Non-contrast-enhanced MRI	+		+	
Nuclear medicine imaging				
V/Q scan	+++			
SPECT	++			
PET		T	T	T

+++ Routine use in clinical practice, ++ routine use in clinical practice of PH centers today, + routine use in clinical practice of PH centers in the near future, T use in clinical trials and research

myocardial and lung metabolism in pathophysiological studies and treatment monitoring, its clinical role has yet to be defined. Besides, it may be useful to exclude rare mimics of CTEPH such as medium- to large-vessel vasculitis such as Takayasu arteritis.

Conclusions

Noninvasive imaging techniques play an important role in diagnosis, classification, prognostic evaluation and follow-up of patients with PH (Table 1). While echocardiography, CT and V/Q scans are an integral part of routine work-up of patients with suspected PH according to current guidelines and across centers, innovative new techniques and applications in the field of PH such as 3D echocardiography, dual-energy CT, 4D flow MRI, T1 and extracellular volume fraction mapping, non-contrast-enhanced MRI sequences for perfusion and ventilation assessment, and molecular-targeted PET are emerging. Not only do these techniques provide new insights into pathophysiological processes of the right heart-pulmonary circulation unit, but they also hold tremendous potential in suggesting the presence of PH, classifying the group of PH, assessing the disease severity and evaluating response to treatment. Among the already intensively studied techniques, particularly cardiac cine MRI has been shown to provide added value to established clinical tests such as 6 min walk distance. Selected and evidence-based advanced imaging markers will play an increasing role in clinical routine for patients with known or suspected PH in the near future.

Compliance with ethical standards

Conflict of interest JVC declares the following: Personal fees and funding from Novartis, Siemens, Boehringer Ingelheim, Bayer; Patent "Method of quantitative magnetic resonance lung imaging" EP3107066, US-2016-0367200-A1 22.12.2016. The other authors declare that they have no conflict of interest.

References

1. Galiè N, Humbert M, Vachiery J-L et al (2015) ESC/ERS Guidelines for the diagnosis and treatment of pulmonary hypertension: the Joint Task Force for the Diagnosis and Treatment of Pulmonary Hypertension of the European Society of Cardiology (ESC) and the European Respiratory Society (ERS): endorsed by: Association for European Paediatric and Congenital Cardiology (AEPC), International Society for Heart and Lung Transplantation (ISHLT). Eur Respir J 46(4):903–975
2. D'Alonzo GE, Barst RJ, Ayres SM et al (1991) Survival in patients with primary pulmonary hypertension. Results from a national prospective registry. Ann Intern Med 115(5):343–349

3. Tuder RM, Marecki JC, Richter A, Fijalkowska I, Flores S (2007) Pathology of pulmonary hypertension. Clin Chest Med 28(1):23–42 vii
4. van Riel ACMJ, Opotowsky AR, Santos M et al (2017) Accuracy of echocardiography to estimate pulmonary artery pressures with exercise: a simultaneous invasive-noninvasive comparison. Circ Cardiovasc Imaging 10(4):e005711
5. Coghlan JG, Denton CP, Grünig E et al (2014) Evidence-based detection of pulmonary arterial hypertension in systemic sclerosis: the DETECT study. Ann Rheum Dis 73(7):1340–1349
6. Marra AM, Egenlauf B, Ehlken N et al (2015) Change of right heart size and function by long-term therapy with riociguat in patients with pulmonary arterial hypertension and chronic thromboembolic pulmonary hypertension. Int J Cardiol 195:19–26
7. van de Veerdonk MC, Marcus JT, Westerhof N et al (2015) Signs of right ventricular deterioration in clinically stable patients with pulmonary arterial hypertension. Chest 147(4):1063–1071
8. Batal O, Dardari Z, Costabile C, Gorcsan J, Arena VC, Mathier MA (2015) Prognostic value of pericardial effusion on serial echocardiograms in pulmonary arterial hypertension. Echocardiography 32(10):1471–1476
9. Kylhammar D, Kjellström B, Hjalmarsson C et al (2017) A comprehensive risk stratification at early follow-up determines prognosis in pulmonary arterial hypertension. Eur Heart J. https://doi.org/10.1093/eurheartj/ehx257
10. Hoeper MM, Kramer T, Pan Z et al (2017) Mortality in pulmonary arterial hypertension: prediction by the 2015 European pulmonary hypertension guidelines risk stratification model. Eur Respir J 50(2):1700740
11. Grünig E, Tiede H, Enyimayew EO et al (2013) Assessment and prognostic relevance of right ventricular contractile reserve in patients with severe pulmonary hypertension. Circulation 128(18):2005–2015
12. Ferrara F, Gargani L, Ostenfeld E et al (2017) Imaging the right heart pulmonary circulation unit: insights from advanced ultrasound techniques. Echocardiography 34(8):1216–1231
13. Rudski LG, Lai WW, Afilalo J et al (2010) Guidelines for the echocardiographic assessment of the right heart in adults: a report from the American Society of Echocardiography endorsed by the European Association of Echocardiography, a registered branch of the European Society of Cardiology, and the Canadian Society of Echocardiography. J Am Soc Echocardiogr 23(7):685–713 quiz 786–788
14. Bhave NM, Patel AR, Weinert L et al (2013) Three-dimensional modeling of the right ventricle from two-dimensional transthoracic echocardiographic images: utility of knowledge-based reconstruction in pulmonary arterial hypertension. J Am Soc Echocardiogr 26(8):860–867
15. Grapsa J, O'Regan DP, Pavlopoulos H, Durighel G, Dawson D, Nihoyannopoulos P (2010) Right ventricular remodelling in pulmonary arterial hypertension with three-dimensional echocardiography: comparison with cardiac magnetic resonance imaging. Eur J Echocardiogr 11(1):64–73
16. Li Y, Wang Y, Zhai Z, Guo X, Yang Y, Lu X (2015) Real-time three-dimensional echocardiography to assess right ventricle function in patients with pulmonary hypertension. PLoS ONE 10(6):e0129557
17. Bossone E, Ferrara F, Grünig E (2015) Echocardiography in pulmonary hypertension. Curr Opin Cardiol 30(6):574–586
18. Leibundgut G, Rohner A, Grize L et al (2010) Dynamic assessment of right ventricular volumes and function by real-time three-dimensional echocardiography: a comparison study with magnetic resonance imaging in 100 adult patients. J Am Soc Echocardiogr 23(2):116–126
19. Gerges M, Gerges C, Lang IM (2015) Advanced imaging tools rather than hemodynamics should be the primary approach for diagnosing, following, and managing pulmonary arterial hypertension. Can J Cardiol 31(4):521–528
20. Grünig E, Peacock AJ (2015) Imaging the heart in pulmonary hypertension: an update. Eur Respir Rev 24(138):653–664
21. D'Alto M, Romeo E, Argiento P et al (2015) Pulmonary arterial hypertension: the key role of echocardiography. Echocardiography 32(Suppl 1):S23–S37
22. Haeck MLA, Scherptong RWC, Marsan NA et al (2012) Prognostic value of right ventricular longitudinal peak systolic strain in patients with pulmonary hypertension. Circ Cardiovasc Imaging 5(5):628–636
23. Sachdev A, Villarraga HR, Frantz RP et al (2011) Right ventricular strain for prediction of survival in patients with pulmonary arterial hypertension. Chest 139(6):1299–1309
24. Greiner S, André F, Heimisch M et al (2013) Non-invasive quantification of right ventricular systolic function by echocardiography: a new semi-automated approach. Clin Res Cardiol 102(3):229–235
25. Vitarelli A, Mangieri E, Terzano C et al (2015) Three-dimensional echocardiography and 2D-3D speckle-tracking imaging in chronic pulmonary hypertension: diagnostic accuracy in detecting hemodynamic signs of right ventricular (RV) failure. J Am Heart Assoc 4(3):e001584
26. Truong QA, Massaro JM, Rogers IS et al (2012) Reference values for normal pulmonary artery dimensions by noncontrast cardiac computed tomography: the Framingham Heart Study. Circ Cardiovasc Imaging 5(1):147–154
27. Shen Y, Wan C, Tian P et al (2014) CT-base pulmonary artery measurement in the detection of pulmonary hypertension: a meta-analysis and systematic review. Medicine (Baltimore) 93(27):e256
28. Tan RT, Kuzo R, Goodman LR, Siegel R, Haasler GB, Presberg KW (1998) Utility of CT scan evaluation for predicting pulmonary hypertension in patients with parenchymal lung disease. Medical College of Wisconsin Lung Transplant Group. Chest 113(5):1250–1256
29. Rajaram S, Swift AJ, Capener D et al (2012) Comparison of the diagnostic utility of cardiac magnetic resonance imaging, computed tomography, and echocardiography in assessment of suspected pulmonary arterial hypertension in patients with connective tissue disease. J Rheumatol 39(6):1265–1274
30. Devaraj A, Wells AU, Meister MG, Corte TJ, Wort SJ, Hansell DM (2010) Detection of pulmonary hypertension with multidetector CT and echocardiography alone and in combination. Radiology 254(2):609–616
31. Tanabe Y, Landeras L, Ghandour A, Partovi S, Rajiah P (2018) State-of-the-art pulmonary arterial imaging—part 1. VASA 47:345–359
32. Goerne H, Chaturvedi A, Partovi S, Rajiah P (2018) State-of-the-art pulmonary arterial imaging—part 2. VASA 47:361–375
33. Biesdorf A, Rohr K, Feng D et al (2012) Segmentation and quantification of the aortic arch using joint 3D model-based segmentation and elastic image registration. Med Image Anal 16(6):1187–1201
34. Linguraru MG, Pura JA, Van Uitert RL et al (2010) Segmentation and quantification of pulmonary artery for noninvasive CT assessment of sickle cell secondary pulmonary hypertension. Med Phys 37(4):1522–1532
35. Froelich JJ, Koenig H, Knaak L, Krass S, Klose KJ (2008) Relationship between pulmonary artery volumes at computed tomography and pulmonary artery pressures in patients with- and without pulmonary hypertension. Eur J Radiol 67(3):466–471
36. Melzig C, Wörz S, Egenlauf B et al (2017) B-0570 - Non-invasive estimation of mean pulmonary arterial pressure in suspected pulmonary hypertension based on automated 3D

volumetry of pulmonary CT angiography. SS 704 - Pulmonary vessels and perfusion, European Congress of Radiology, Vienna
37. Jivraj K, Bedayat A, Sung YK et al (2017) Left atrium maximal axial cross-sectional area is a specific computed tomographic imaging biomarker of World Health Organization Group 2 pulmonary hypertension. J Thorac Imaging 32(2):121–126
38. Currie BJ, Johns C, Chin M et al (2018) CT derived left atrial size identifies left heart disease in suspected pulmonary hypertension: derivation and validation of predictive thresholds. Int J Cardiol 260:172–177
39. Aviram G, Rozenbaum Z, Ziv-Baran T et al (2017) Identification of pulmonary hypertension caused by left-sided heart disease (World Health Organization Group 2) based on cardiac chamber volumes derived from chest CT imaging. Chest 152(4):792–799
40. Nakazawa T, Watanabe Y, Hori Y et al (2011) Lung perfused blood volume images with dual-energy computed tomography for chronic thromboembolic pulmonary hypertension: correlation to scintigraphy with single-photon emission computed tomography. J Comput Assist Tomogr 35(5):590–595
41. Hachulla A-L, Lador F, Soccal PM, Montet X, Beghetti M (2016) Dual-energy computed tomographic imaging of pulmonary hypertension. Swiss Med Wkly 146:w14328
42. Koike H, Sueyoshi E, Sakamoto I, Uetani M, Nakata T, Maemura K (2018) Comparative clinical and predictive value of lung perfusion blood volume CT, lung perfusion SPECT and catheter pulmonary angiography images in patients with chronic thromboembolic pulmonary hypertension before and after balloon pulmonary angioplasty. Eur Radiol. https://doi.org/10.1007/s00330-018-5501-4
43. Ameli-Renani S, Ramsay L, Bacon JL et al (2014) Dual-energy computed tomography in the assessment of vascular and parenchymal enhancement in suspected pulmonary hypertension. J Thorac Imaging 29(2):98–106
44. Leithner D, Wichmann JL, Vogl TJ et al (2017) Virtual monoenergetic imaging and iodine perfusion maps improve diagnostic accuracy of dual-energy computed tomography pulmonary angiography with suboptimal contrast attenuation. Invest Radiol 52(11):659–665
45. McLure LER, Peacock AJ (2009) Cardiac magnetic resonance imaging for the assessment of the heart and pulmonary circulation in pulmonary hypertension. Eur Respir J 33(6):1454–1466
46. Grothues F, Smith GC, Moon JCC et al (2002) Comparison of interstudy reproducibility of cardiovascular magnetic resonance with two-dimensional echocardiography in normal subjects and in patients with heart failure or left ventricular hypertrophy. Am J Cardiol 90(1):29–34
47. Kawel-Boehm N, Maceira A, Valsangiacomo-Buechel ER et al (2015) Normal values for cardiovascular magnetic resonance in adults and children. J Cardiovasc Magn Reson 17:29
48. Swift AJ, Capener D, Johns C et al (2017) Magnetic resonance imaging in the prognostic evaluation of patients with pulmonary arterial hypertension. Am J Respir Crit Care Med 196(2):228–239
49. van Wolferen SA, Marcus JT, Boonstra A et al (2007) Prognostic value of right ventricular mass, volume, and function in idiopathic pulmonary arterial hypertension. Eur Heart J 28(10):1250–1257
50. Peacock AJ, Crawley S, McLure L et al (2014) Changes in right ventricular function measured by cardiac magnetic resonance imaging in patients receiving pulmonary arterial hypertension-targeted therapy: the EURO-MR study. Circ Cardiovasc Imaging 7(1):107–114
51. Freed BH, Collins JD, François CJ et al (2016) MR and CT imaging for the evaluation of pulmonary hypertension. JACC Cardiovasc Imaging 9(6):715–732
52. Roeleveld RJ, Marcus JT, Faes TJC et al (2005) Interventricular septal configuration at mr imaging and pulmonary arterial pressure in pulmonary hypertension. Radiology 234(3):710–717
53. Swift AJ, Rajaram S, Hurdman J et al (2013) Noninvasive estimation of PA pressure, flow, and resistance with CMR imaging: derivation and prospective validation study from the ASPIRE registry. JACC Cardiovasc Imaging 6(10):1036–1047
54. Johns CS, Rajaram S, Capener DA et al (2018) Non-invasive methods for estimating mPAP in COPD using cardiovascular magnetic resonance imaging. Eur Radiol 28(4):1438–1448
55. Shehata ML, Cheng S, Osman NF, Bluemke DA, Lima JAC (2009) Myocardial tissue tagging with cardiovascular magnetic resonance. J Cardiovasc Magn Reson 11:55
56. Shehata ML, Basha TA, Tantawy WH et al (2010) Real-time single-heartbeat fast strain-encoded imaging of right ventricular regional function: normal versus chronic pulmonary hypertension. Magn Reson Med 64(1):98–106
57. Shehata ML, Harouni AA, Skrok J et al (2013) Regional and global biventricular function in pulmonary arterial hypertension: a cardiac MR imaging study. Radiology 266(1):114–122
58. Maschke SK, Schoenfeld CO, Kaireit TF et al (2018) MRI-derived regional biventricular function in patients with chronic thromboembolic pulmonary hypertension before and after pulmonary endarterectomy. Acad Radiol. https://doi.org/10.1016/j.acra.2018.04.002
59. Barker AJ, Roldán-Alzate A, Entezari P et al (2015) Four-dimensional flow assessment of pulmonary artery flow and wall shear stress in adult pulmonary arterial hypertension: results from two institutions. Magn Reson Med 73(5):1904–1913
60. Delles M, Rengier F, Azad Y-J et al (2015) Non-invasive pulmonary blood flow analysis and blood pressure mapping derived from 4D flow MRI. Proc SPIE 9417:94172G
61. Rengier F, Delles M, Eichhorn J et al (2015) Noninvasive 4D pressure difference mapping derived from 4D flow MRI in patients with repaired aortic coarctation: comparison with young healthy volunteers. Int J Cardiovasc Imaging 31(4):823–830
62. Reiter G, Reiter U, Kovacs G, Olschewski H, Fuchsjäger M (2015) Blood flow vortices along the main pulmonary artery measured with MR imaging for diagnosis of pulmonary hypertension. Radiology 275(1):71–79
63. Rengier F, Geisbüsch P, Schoenhagen P et al (2014) State-of-the-art aortic imaging: part II—applications in transcatheter aortic valve replacement and endovascular aortic aneurysm repair. VASA 43(1):6–26
64. Tang BT, Pickard SS, Chan FP, Tsao PS, Taylor CA, Feinstein JA (2012) Wall shear stress is decreased in the pulmonary arteries of patients with pulmonary arterial hypertension: an image-based, computational fluid dynamics study. Pulm Circ 2(4):470–476
65. Kheyfets VO, Rios L, Smith T et al (2015) Patient-specific computational modeling of blood flow in the pulmonary arterial circulation. Comput Methods Progr Biomed 120(2):88–101
66. Vogel-Claussen J, Rochitte CE, Wu KC et al (2006) Delayed enhancement MR imaging: utility in myocardial assessment. Radiographics 26(3):795–810
67. Shehata ML, Lossnitzer D, Skrok J et al (2011) Myocardial delayed enhancement in pulmonary hypertension: pulmonary hemodynamics, right ventricular function, and remodeling. AJR Am J Roentgenol 196(1):87–94
68. Bessa LGP, Junqueira FP, Bandeira MLDS et al (2013) Pulmonary arterial hypertension: use of delayed contrast-enhanced cardiovascular magnetic resonance in risk assessment. Arq Bras Cardiol 101(4):336–343
69. Junqueira FP, Macedo R, Coutinho AC et al (2009) Myocardial delayed enhancement in patients with pulmonary hypertension and right ventricular failure: evaluation by cardiac MRI. Br J Radiol 82(982):821–826

70. Sanz J, Dellegrottaglie S, Kariisa M et al (2007) Prevalence and correlates of septal delayed contrast enhancement in patients with pulmonary hypertension. Am J Cardiol 100(4):731–735
71. McCann GP, Gan CT, Beek AM, Niessen HWM, Vonk Noordegraaf A, van Rossum AC (2007) Extent of MRI delayed enhancement of myocardial mass is related to right ventricular dysfunction in pulmonary artery hypertension. AJR Am J Roentgenol 188(2):349–355
72. McLaughlin VV, Sitbon O, Badesch DB et al (2005) Survival with first-line bosentan in patients with primary pulmonary hypertension. Eur Respir J 25(2):244–249
73. Messroghli DR, Moon JC, Ferreira VM et al (2017) Clinical recommendations for cardiovascular magnetic resonance mapping of T1, T2, T2* and extracellular volume: a consensus statement by the Society for Cardiovascular Magnetic Resonance (SCMR) endorsed by the European Association for Cardiovascular Imaging (EACVI). J Cardiovasc Magn Reson 19(1):75
74. Messroghli DR, Radjenovic A, Kozerke S, Higgins DM, Sivananthan MU, Ridgway JP (2004) Modified look-locker inversion recovery (MOLLI) for high-resolution T1 mapping of the heart. Magn Reson Med 52(1):141–146
75. Messroghli DR, Walters K, Plein S et al (2007) Myocardial T1 mapping: application to patients with acute and chronic myocardial infarction. Magn Reson Med 58(1):34–40
76. Mehta BB, Chen X, Bilchick KC, Salerno M, Epstein FH (2015) Accelerated and navigator-gated look-locker imaging for cardiac T1 estimation (ANGIE): development and application to T1 mapping of the right ventricle. Magn Reson Med 73(1):150–160
77. Mehta BB, Auger DA, Gonzalez JA et al (2015) Detection of elevated right ventricular extracellular volume in pulmonary hypertension using accelerated and navigator-gated look-locker imaging for cardiac T1 estimation (ANGIE) cardiovascular magnetic resonance. J Cardiovasc Magn Reson 17:110
78. Roller FC, Wiedenroth C, Breithecker A et al (2017) Native T1 mapping and extracellular volume fraction measurement for assessment of right ventricular insertion point and septal fibrosis in chronic thromboembolic pulmonary hypertension. Eur Radiol 27(5):1980–1991
79. García-Álvarez A, García-Lunar I, Pereda D et al (2015) Association of myocardial T1-mapping CMR with hemodynamics and RV performance in pulmonary hypertension. JACC Cardiovasc Imaging 8(1):76–82
80. Partovi S, Aschwanden M, Staub D et al (2011) Gadofosveset enhanced MR phlebography for detecting pelvic and deep vein leg thrombosis. VASA 40(4):315–319
81. Stein PD, Chenevert TL, Fowler SE et al (2010) Gadolinium-enhanced magnetic resonance angiography for pulmonary embolism: a multicenter prospective study (PIOPED III). Ann Intern Med 152(7):434–443 W142–W143
82. Sostman HD, Jablonski KA, Woodard PK et al (2012) Factors in the technical quality of gadolinium enhanced magnetic resonance angiography for pulmonary embolism in PIOPED III. Int J Cardiovasc Imaging 28(2):303–312
83. Pengo V, Lensing AWA, Prins MH et al (2004) Incidence of chronic thromboembolic pulmonary hypertension after pulmonary embolism. N Engl J Med 350(22):2257–2264
84. Olsson KM, Meyer B, Hinrichs J, Vogel-Claussen J, Hoeper MM, Cebotari S (2014) Chronic thromboembolic pulmonary hypertension. Dtsch Arztebl Int 111(50):856–862
85. Ohno Y, Koyama H, Yoshikawa T et al (2012) Contrast-enhanced multidetector-row computed tomography vs. time-resolved magnetic resonance angiography vs. contrast-enhanced perfusion MRI: assessment of treatment response by patients with inoperable chronic thromboembolic pulmonary hypertension. J Magn Reson Imaging 36(3):612–623
86. Sourbron S, Luypaert R, Morhard D, Seelos K, Reiser M, Peller M (2007) Deconvolution of bolus-tracking data: a comparison of discretization methods. Phys Med Biol 52(22):6761–6778
87. Hueper K, Parikh MA, Prince MR et al (2013) Quantitative and semiquantitative measures of regional pulmonary microvascular perfusion by magnetic resonance imaging and their relationships to global lung perfusion and lung diffusing capacity: the multi-ethnic study of atherosclerosis chronic obstructive pulmonary disease study. Invest Radiol 48(4):223–230
88. Schoenfeld C, Cebotari S, Hinrichs J et al (2016) MR imaging-derived regional pulmonary parenchymal perfusion and cardiac function for monitoring patients with chronic thromboembolic pulmonary hypertension before and after pulmonary endarterectomy. Radiology 279(3):925–934
89. Prybylski JP, Semelka RC, Jay M (2017) The stability of gadolinium-based contrast agents in human serum: a reanalysis of literature data and association with clinical outcomes. Magn Reson Imaging 38:145–151
90. Huckle JE, Altun E, Jay M, Semelka RC (2016) Gadolinium deposition in humans: when did we learn that gadolinium was deposited in vivo? Invest Radiol 51(4):236–240
91. Gulani V, Calamante F, Shellock FG, Kanal E, Reeder SB, International Society for Magnetic Resonance in Medicine (2017) Gadolinium deposition in the brain: summary of evidence and recommendations. Lancet Neurol 16(7):564–570
92. Rengier F, Geisbüsch P, Vosshenrich R et al (2013) State-of-the-art aortic imaging: part I—fundamentals and perspectives of CT and MRI. VASA 42(6):395–412
93. Edelman RR, Silvers RI, Thakrar KH et al (2017) Nonenhanced MR angiography of the pulmonary arteries using single-shot radial quiescent-interval slice-selective (QISS): a technical feasibility study. J Cardiovasc Magn Reson 19(1):48
94. Bannas P, Bell LC, Johnson KM et al (2016) Pulmonary embolism detection with three-dimensional ultrashort echo time MR imaging: experimental study in canines. Radiology 278(2):413–421
95. Bauman G, Puderbach M, Deimling M et al (2009) Non-contrast-enhanced perfusion and ventilation assessment of the human lung by means of fourier decomposition in proton MRI. Magn Reson Med 62(3):656–664
96. Voskrebenzev A, Gutberlet M, Becker L, Wacker F, Vogel-Claussen J (2016) Reproducibility of fractional ventilation derived by Fourier decomposition after adjusting for tidal volume with and without an MRI compatible spirometer. Magn Reson Med 76(5):1542–1550
97. Fischer A, Weick S, Ritter CO et al (2014) SElf-gated non-contrast-enhanced functional lung imaging (SENCEFUL) using a quasi-random fast low-angle shot (FLASH) sequence and proton MRI. NMR Biomed 27(8):907–917
98. Bauman G, Lützen U, Ullrich M et al (2011) Pulmonary functional imaging: qualitative comparison of Fourier decomposition MR imaging with SPECT/CT in porcine lung. Radiology 260(2):551–559
99. Bauman G, Scholz A, Rivoire J et al (2013) Lung ventilation- and perfusion-weighted Fourier decomposition magnetic resonance imaging: in vivo validation with hyperpolarized 3He and dynamic contrast-enhanced MRI. Magn Reson Med 69(1):229–237
100. Schönfeld C, Cebotari S, Voskrebenzev A et al (2015) Performance of perfusion-weighted Fourier decomposition MRI for detection of chronic pulmonary emboli. J Magn Reson Imaging 42(1):72–79
101. Fedullo PF, Auger WR, Kerr KM, Rubin LJ (2001) Chronic thromboembolic pulmonary hypertension. N Engl J Med 345(20):1465–1472

102. Tunariu N, Gibbs SJR, Win Z et al (2007) Ventilation-perfusion scintigraphy is more sensitive than multidetector CTPA in detecting chronic thromboembolic pulmonary disease as a treatable cause of pulmonary hypertension. J Nucl Med 48(5):680–684
103. Lu Y, Lorenzoni A, Fox JJ et al (2014) Noncontrast perfusion single-photon emission CT/CT scanning: a new test for the expedited, high-accuracy diagnosis of acute pulmonary embolism. Chest 145(5):1079–1088
104. Derlin T, Kelting C, Hueper K et al (2018) Quantitation of perfused lung volume using hybrid SPECT/CT allows refining the assessment of lung perfusion and estimating disease extent in chronic thromboembolic pulmonary hypertension. Clin Nucl Med 43(6):e170–e177
105. Burger IA, Husmann L, Herzog BA et al (2011) Main pulmonary artery diameter from attenuation correction CT scans in cardiac SPECT accurately predicts pulmonary hypertension. J Nucl Cardiol 18(4):634–641
106. Wang L, Li W, Yang Y et al (2016) Quantitative assessment of right ventricular glucose metabolism in idiopathic pulmonary arterial hypertension patients: a longitudinal study. Eur Heart J Cardiovasc Imaging 17(10):1161–1168
107. Oikawa M, Kagaya Y, Otani H et al (2005) Increased [18F] fluorodeoxyglucose accumulation in right ventricular free wall in patients with pulmonary hypertension and the effect of epoprostenol. J Am Coll Cardiol 45(11):1849–1855
108. Saygin D, Highland KB, Farha S et al (2017) Metabolic and functional evaluation of the heart and lungs in pulmonary hypertension by gated 2-[18F]-fluoro-2-deoxy-D-glucose positron emission tomography. Pulm Circ 7(2):428–438
109. Kluge R, Barthel H, Pankau H et al (2005) Different mechanisms for changes in glucose uptake of the right and left ventricular myocardium in pulmonary hypertension. J Nucl Med 46(1):25–31
110. Tatebe S, Fukumoto Y, Oikawa-Wakayama M et al (2014) Enhanced [18F]fluorodeoxyglucose accumulation in the right ventricular free wall predicts long-term prognosis of patients with pulmonary hypertension: a preliminary observational study. Eur Heart J Cardiovasc Imaging 15(6):666–672
111. Fang W, Zhao L, Xiong C-M et al (2012) Comparison of 18F-FDG uptake by right ventricular myocardium in idiopathic pulmonary arterial hypertension and pulmonary arterial hypertension associated with congenital heart disease. Pulm Circ 2(3):365–372
112. Zhao L, Ashek A, Wang L et al (2013) Heterogeneity in lung (18)FDG uptake in pulmonary arterial hypertension: potential of dynamic (18)FDG positron emission tomography with kinetic analysis as a bridging biomarker for pulmonary vascular remodeling targeted treatments. Circulation 128(11):1214–1224
113. Marsboom G, Wietholt C, Haney CR et al (2012) Lung ^{18}F-fluorodeoxyglucose positron emission tomography for diagnosis and monitoring of pulmonary arterial hypertension. Am J Respir Crit Care Med 185(6):670–679
114. Ohira H, de Kemp R, Pena E et al (2016) Shifts in myocardial fatty acid and glucose metabolism in pulmonary arterial hypertension: a potential mechanism for a maladaptive right ventricular response. Eur Heart J Cardiovasc Imaging 17(12):1424–1431